Kazumasa Oguri[1,2], Pere Masqué[3,4,5], Matthias Zabel[6], Heather A. Stewart[7], Gillian MacKinnon[8], Ashley A. Rowden[9,10], Frank Wenzhöfer[1,11,12], Ronnie N. Glud[1,13,14]

[1] Hadal & Nordcee, Department of Biology, University of Southern Denmark, 5230 Odense M, Denmark

[2] Research Institute for Global Change, Japan Agency for Marine-Earth Science and Technology, 2-15 Natsushima-cho, Yokosuka, 237-0061 Japan

[3] School of Natural Sciences, Centre for Marine Ecosystems Research, Edith Cowan University, Joondalup, WA, Australia

[4] Institute of Environmental Science and Technology and Physics Department, Universitat Autònoma de Barcelona, Bellaterra, Spain

[5] International Atomic Energy Agency Environment Laboratories, 4, Quai Antoine 1er 98000 Monaco

[6] Center for Marine Environmental Sciences, University of Bremen, Leobener Str. 8, D-28359 Bremen, Germany

[7] British Geological Survey, Lyell Centre, Research Avenue South, Edinburgh, EH14 4AP, UK

[8] Scottish Universities Environmental Research Centre, Scottish Enterprise Technology Park, East Kilbride, South Lanarkshire, G75 OQF, UK

[9] National Institute of Water & Atmosphere Research (NIWA), Private Bag 14901, Wellington, New Zealand

[10] Victoria University of Wellington, PO Box 600, Wellington, New Zealand

[11] HGF-MPG Group for Deep Sea Ecology and Technology, Alfred-Wegener-Institute Helmholtz-Center for Polar and Marine Research, 27570 Bremerhaven, Germany

[12] Max Planck Institute for Marine Microbiology, 28359 Bremen, Germany

[13] Tokyo University of Marine Science and Technology, 4-5-7 Konan, Minato-ku, Tokyo, 108-8477, Japan

[14] DIAS, University of Southern Denmark, 5230 Odense M, Denmark

Corresponding author: Kazumasa Oguri (ogurik@biology.sdu.dk)

**Key Points**

- Hadal trench systems act as important hot spots for accumulation and retention of organic material in the deep sea.
- The sediment and organic carbon accumulation in trench systems are partly mediated by material focusing but mainly by mass-wasting events.

- Sediment and organic carbon deposition rates vary within and between trench systems due to sporadic seismic activity and local bathymetry.

**Abstract**

Hadal trenches act as depocenters for organic material, although pathways for hadal material transport and deposition rates are poorly constrained. Here we assess, focusing, deposition and accumulation, of material and organic carbon in four hadal trench systems underlying provinces of different net primary productivity in the surface ocean – from the eutrophic Atacama and Kuril-Kamchatka trenches, and the mesotrophic Kermadec Trench, to the oligotrophic Mariana Trench. The study is based on the distributions of $^{210}Pb_{ex}$, $^{137}Cs$ and total organic carbon from recovered sediment cores and by applying previously quantified benthic mineralization rates. Periods of steady deposition and discreet mass-wasting deposits were identified from the profiles and the latter were associated with historic recorded seismic events in the respective regions. During periods without mass wasting, the estimated focusing factors along trench axes were elevated, suggesting continuous downslope focusing of material towards the interior of the trenches. The estimated accumulation rates of organic carbon during these periods exhibited extensive site-specific variability but were generally similar to values encountered at much shallower settings such as continental slopes and margins. Organic carbon deposition and accumulation rates during periods of steady deposition was not mirrored by surface ocean productivity, but appeared confounded by local bathymetry. Seismic driven mass wasting events markedly enhanced the accumulation of sediment and organic carbon by factors from 20 to 400. Thus, hadal trenches are important sites for deposition and sequestration of organic carbon in the deep-sea partly due to intensified downslope focusing of material but mainly due to mass-wasting events.

**Plain Language Summary**

Hadal trenches (>6000 m water depth) occupy ~1 % of the world's ocean bed yet are underexplored, but recent studies have shown that these environments are depocenters for organic material and microbial activity is intensified when compared to shallower abyssal plains. However, transport and accumulation of sediment material to these hadal trenches is poorly understood. This study investigates sedimentation and accumulation dynamics of organic carbon in trenches using results of radionuclide analysis (in sediment from the Atacama, Kuril-Kamchatka, Kermadec, and Mariana trenches. The analysis shows that trench sediments consist of discreet layers representing both periods of continuous deposition and sudden mass-wasting events often triggered by historic earthquakes. Down slope focusing of material intensified deposition along the trench axes. However, the rates exhibited extensive site-specific variations that partly were related to mass-wasting events which greatly enhanced not only mass accumulation but also organic carbon accumulation in the trench axes. Our results illustrate the important role that mass-wasting events of supplying organic carbon to hadal communities and suggest that hadal trenches might be quantitatively important for sediment and organic carbon sequestration in the

deep sea.

**Keywords:**

Hadal trench, radionuclides, mass accumulation rate, focusing factor, mass-wasting event, organic carbon accumulation rate

## 1. Introduction

The hadal zone is defined as regions with water depths exceeding 6000 m and covers approximately 1 % of the ocean floor (Harris et al., 2014). The most prominent hadal environments stretch along tectonic subduction zones, where they form long, narrow trench systems. Generally, the vertical transport of organic material from the surface ocean attenuates strongly with ocean depth (Berger et al. 1987), but during the past two decades it has been realized that hadal trenches can act as depocenters for organic material (Danovaro et al., 2003; Ichino et al., 2015; Xu et al., 2021). In addition, some trench sediments hold surprisingly high levels of microbial and meiofaunal biomass (e.g., Itoh et al., 2011; Brandt et al., 2020; Schauberger et al., 2021) and hadal sediments appear to express elevated $O_2$ consumption rates as compared to adjacent abyssal sites with water depths of 5000-6000 m (Glud et al., 2013; Wenzhöfer et al., 2016; Luo et al., 2019; Glud et al., 2021). These observations imply that deposited organic materials in trenches not only consist of resilient pre-aged organic material but include relatively labile and nutritious organics that can sustain highly active biological communities thriving at extreme hydrostatic pressure. Indeed, high but variable concentrations of phytodetrital material has been found in hadal sediments (Glud et al., 2013; Wenzhöfer et al., 2016) and deposition in hadal environments appears to be modulated by several processes.

Tidal fluid dynamics may induce internal waves which combined with complex seafloor bathymetry have been suggested to focus (and winnow) relatively fresh material along trench axes (Turnewitsch et al., 2014; van Haren, 2020). This focusing/winnowing of deposited organic material would partly explain the extensive spatial variability in microbial activity encountered along trench axes despite relatively similar surface ocean production (Glud et al., 2021). However, hadal subduction trenches are located at plate boundaries and are exposed to frequent earthquakes that may trigger mass-wasting events (Nozaki & Ohta, 1993; Oguri et al., 2013; Ikehara et al., 2016; Bao et al., 2018; Usami et al., 2018) that re-distribute sedimentary and organic materials from the trench slope towards the trench axis (Kawamura et al., 2012**;** McHugh et al., 2020). For example, the Tohoku-Oki earthquake ($M_w$=9.1) in 2011, is estimated to have remobilized more than 1 Tg of carbon towards the axis of the Japan Trench (Kioka et al., 2019a). Past mass-wasting events are preserved in the sedimentary record and are often characterized by layers of abnormal age distribution of organic material as determined by $^{14}C$ dating ($^{14}C_{OC}$), with older deposits overlying younger and fresher material (Bao et al., 2018; Ikehara et al., 2020; Usami et al., 2021; Xu et al. 2021). The rapid re-deposition may also form unusual thick sediment layers characterized by high levels of excess $^{210}Pb$ ($^{210}Pb_{ex}$) along the trench

axes (Oguri et al., 2013; McHugh et al., 2016; 2020). However, mass-wasting events may not only redeposit large amounts of organic carbon from the slopes towards the trench axes but may also carry, and focus, relatively fresh phytodetrital material (Oguri et al., 2013) and carrion killed during these catastrophic events (Arai et al., 2013; Oguri et al., 2013).

Hadal trenches remain grossly under sampled and the extent that deposited organic material is retained in the sedimentary record or mineralized remain poorly constrained. Here we quantify deposition dynamics in four different hadal trench systems from the distribution of radionuclides ($^{210}Pb_{ex}$ and $^{137}Cs$) in recovered sediment cores. The study areas underlie oceanic provinces of highly different surface ocean production – from the eutrophic, Atacama, and Kuril-Kamchatka trenches to the mesotrophic Kermadec Trench and the oligotrophic Mariana Trench. These data are used to quantify sedimentation and mass accumulation rates, material focusing and accumulation efficiency of organic carbon at the axis of the four targeted trench systems.

## 2. Methods

### 2.1. Sediment sampling and storage

Sediment cores within the four targeted trench systems (Figure 1a), were collected during the cruises of R/V Sonne (Atacama Trench, SO261 from 2/Mar to 2/Apr/2018; Figure 1b), R/V Sonne (Kuril-Kamchatka Trench, SO250 from 16/Aug to 26/Sep/2016; Figure 1c), R/V Tangaroa (Kermadec Trench, TAN1711 from 24/Nov to 14/Dec/2017; Figure 1d), and R/V Yokosuka (Mariana Trench, YK10-16 from 20/Nov to 4/Dec/2010; Figure 1e). Summary information on the sampling sites is provided in Table 1. Most sediment cores were collected with a multi-corer (Barnett et al., 1984), two sites were sampled with a box corer and three sites were sampled by an autonomous sediment coring lander (Table 1). The sediment cores were quickly transferred to a thermo-regulated room maintaining temperature close to *in situ* conditions. Within 24 hours, the cores were sectioned, and each sediment slice was homogenized and kept frozen in plastic bags until analysis.

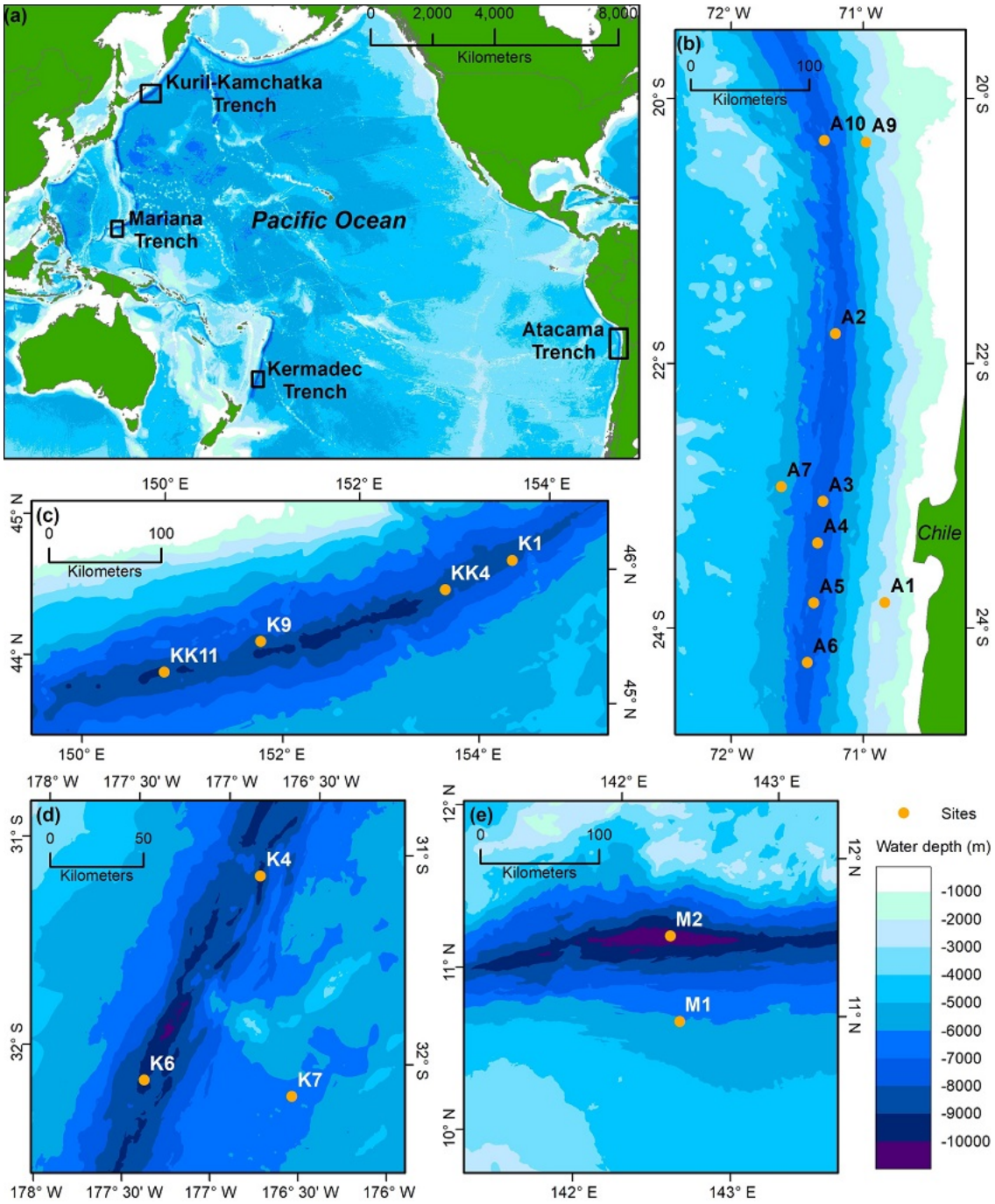


**Figure 1.** (a) Location of the four trench systems targeted by the study: Atacama, Kuril-Kamchatka, Kermadec and Mariana trenches. Sampling sites in the

individual trench regions are depicted in the subpanels; (b) Atacama, (c) Kuril-Kamchatka, (d) Kermadec, and (e) Mariana. All elevation data sourced from the GEBCO Compilation Group (2021). 

**Table 1.** Sampling Sites, Water Depth, Latitude, Longitude, Core Length and Sampling Equipment.

*Note.* MUC: multi-corer, and BC: box corer. Net primary productivity where derived from a model of Behrenfeld & Falkowski (2007) and remote sensing data from the period 2009-2018 at the respective sites. The values of Atacama, Kermadec and Mariana Trenches have previously been presented in Glud et al. (2021). Precise depth, latitude, longitude may be slightly varied by correction from the ship positioning. For detail, please contact to the author.

In the onshore laboratory wet re-homogenized sediment was transferred to a plastic cube of known internal volume. The sediment weight was determined before and after drying the samples at 80°C for a total of 48 hours to calculate the water content and the dry bulk density. Subsequently the material was ground into powder with an agate mortar and pestle in preparation for measurements of the concentration of the targeted radionuclides.

### 2.2. Measurements of $^{210}Pb_{ex}$ and $^{137}Cs$ concentrations and calculations of sedimentation and mass accumulation rates.

Recent (~100 years) deposition dynamics, and sedimentation and mass accumulation rates (SR and MAR) can be derived from the sedimentary distribution of excess $^{210}Pb$ ($^{210}Pb_{ex}$; half-life of 22.3 years) (Koide et al. 1972). The particle reactive $^{210}Pb_{ex}$ is produced from decay of $^{222}Rn$ in the atmosphere and the water column and accumulates at the sediment surface via particle scavenging (Craig et al., 1972; Koide et al., 1972). Non-bioturbated sediment characterized by slow and steady accumulations exhibit $^{210}Pb_{ex}$ profiles with a mono exponential decline from the surface layer, while layers deposited during mass-wasting events are identified as layers of constant $^{210}Pb_{ex}$. In addition, $^{137}Cs$ (half-life of 30 years) originating from previous nuclear tests in the Northern Hemisphere and catastrophic accidents at nuclear power plants, represent another chronological indicator for recent (after 1955) deposition dynamics (e.g., Fuller et al., 1999; Kusakabe et al., 2017).

The analyses of $^{210}Pb_{ex}$ and $^{137}Cs$ in the sediment samples from Atacama, Kermadec and Mariana trenches were carried out at Japan Agency for Marine-Earth Science and Technology (JAMSTEC), while samples from Kuril-Kamchatka Trench were analyzed at The Scottish Universities Environmental Research Centre (SUERC). At both institutions, the radionuclide concentrations were quantified by gamma spectrometry. For 5 sites in the Atacama Trenches (A1, A2,

A4, A5 and A6), the $^{210}Pb_{ex}$ profiles were also quantified in parallel at Edith Cowan University (ECU, Australia).

At JAMSTEC, 2.0 g of sediment was placed in a sealed plastic vessel and kept for at least 2 months to establish secular equilibrium between $^{226}Ra$ and $^{222}Rn$. For gamma ray counting, well-type High-Purity Germanium (HPGe) detectors (GWL120230 or GWL120-15, ORTEC-Ametek). Samples were counted for 1 to 4 days. The emission peaks of $^{210}Pb$, $^{214}Pb$ and $^{137}Cs$ used for the analysis were 46.5, 351.9 and 661.6 keV, respectively. The $^{210}Pb_{ex}$ concentrations were calculated by subtracting the $^{214}Pb$ concentrations from the total $^{210}Pb$. In case two-standard deviations of the mean $^{210}Pb_{ex}$ reached negative values, the mean was considered below background and removed from the dataset.

At ECU, the $^{210}Pb$ concentrations were determined through the analysis of the concentration of its granddaughter $^{210}Po$ by alpha-spectroscopy, assuming secular equilibrium of both radionuclides at the time of analysis (Sanchez-Cabeza et al., 1998). Samples were traced using $^{209}Po$, followed by an acid digestion using an analytical microwave, and polonium isotopes were subsequently plated on silver discs. Alpha emissions were quantified using Passivated Implanted Planar Silicon (PIPS) detectors (Model PD-450.18 A.M., Canberra) with a Maestro$^{TM}$ data acquisition software. Some samples from each core were measured by gamma spectrometry to quantify the specific concentrations of $^{226}Ra$ through the emission lines of its decay product $^{214}Pb$ (295.2 and 351.9 keV) using calibrated geometries in a HPGe detector (Model SAGe Well, Canberra). The analysis at ECU and JAMSTEC were conducted on separate cores sampled in the same multi-corer casts, and thus recovered within 1 m distance on the seabed.

At SUERC, 5.5 to 20.6 g of dried sediment powders were pressed (10-12 tons of pressure applied using an Enerpac hydraulic disc press) into uniform geometries and the pellets placed into a 55 mm diameter petri dish and sealed with epoxy resin. The sealed samples were then stored for a minimum of three weeks before counting to ensure equilibrium between $^{226}Ra$ and $^{222}Rn$. Measurements were made using a low background Profile series HPGe Coaxial photon detector (GEM-S-XLB-C, ORTEC-Ametek). Analysis times ranged between 1-9 days. Concentrations of the samples were calculated relative to background measurements and the standard materials in the same geometry to correct for geometry and self-absorption.

SR (in mm $y^{-1}$) and MAR (in g $cm^{-2}$ $y^{-1}$) were calculated from sections of the $^{210}Pb_{ex}$ profiles indicating mono exponential declines in concentrations and thus excluded the contribution of deposition during mass-wasting events as identified by constant $^{210}Pb_{ex}$ across distinct depth intervals. The MAR were estimated using the Constant Flux:Constant Sedimentation (CF:CS) model (Krishnaswami et al., 1971). Total MAR including contributions from mass wasting were derived from the total inventory of $^{210}Pb_{ex}$ as described in section 2.3.

### 2.3. Calculation of pelagic focusing factors

To independently assess material focusing along the trench axes, we derived a focusing factor, expressing the ratio between the $^{210}Pb_{ex}$ inventory in the sediment and the calculated pelagic deficit of the $^{210}Pb$ inventory in the water column (Kato et al., 2003; Turnewitsch et al., 2004). Assuming steady state, no horizontal material transport and no addition of $^{210}Pb_{ex}$ from subsurface sediment layers, the $^{210}Pb$ deficient of the pelagic inventory should be equivalent to the $^{210}Pb_{ex}$ inventory and the corresponding focusing factor would thus amount to 1.0. Values above 1.0 or below 1.0 would suggest focusing or winnowing of material, respectively. The $^{210}Pb_{ex}$ inventory in sediments were calculated from the following equation:

$$I = \sum A \bullet z \bullet DBD \quad (1)$$

where $I$=$^{210}Pb_{ex}$ inventory (Bq cm$^{-2}$), A= $^{210}Pb_{ex}$ concentration (Bq g$^{-1}$) in the targeted sediment horizon of thickness z (cm) and DBD= dry bulk density of the sediment (g cm$^{-3}$) at z. In this study, we derived two values for the $^{210}Pb_{ex}$ inventories, either including or excluding the sediment layers considered to have deposited during mass-wasting events. In the cores collected from the abyssal plains in the Atacama and Kermadec trenches (A7 and K7), the seabed was covered by manganese nodules. Manganese nodules are known to elevate $^{210}Pb_{ex}$ concentration in the upper sediment layers by the release of $^{222}Rn$ (DeMaster & Cochran, 1982). Therefore, the $^{210}Pb_{ex}$ inventories for these sites were derived from the mono exponential decline until reaching low background levels assuming a general profile off-set as argued by DeMaster & Cochran (1982).

Deficits of $^{210}Pb$ inventory in the pelagic realm was calculated by subtracting the $^{210}Pb$ inventory from the $^{226}Ra$ inventory in the water column. The pelagic inventories of both nuclides were obtained from profiles measured by previous studies at sites close to our benthic sites (Chung & Craig, 1973; Thomson & Turekian, 1976; Chung & Craig, 1980; 1983). The positions of these sites and the distance between pelagic and benthic sites ranged between 410 and 2600 km (Table S1). The $^{210}Pb$ and $^{226}Ra$ concentrations below the maximal measuring depth were extrapolated to the sea floor assuming constant concentrations (Turnewitsch et al., 2014).

### 2.4. Measurement of total organic carbon (TOC) content and organic carbon deposition rates.

The TOC content of Atacama, Kermadec and Mariana trench samples were measured at University of Southern Denmark (SDU), and Kuril-Kamchatka Trench samples were measured at the Scottish Association for Marine Science (SAMS), respectively. AT SDU, sediment samples were first acidified, dried and milled. Then these samples were placed in small tin capsules that were transferred to an elemental analyzer (Delta V Advantage, Thermo scientific). TOC contents were derived from parallel sediment cores collected during the same multi-corer cast. At SAMS, sediment samples were dried and milled after decalcification with 5 % sulphuric acid. The samples processed were enclosed in tin capsules, and the contents were measured with an elemental analyzer (Elemental Com-

bustion ECS4010, Costech). To estimate the analytical precision, triplicates of every 5-10th sample were measured. Accuracy of analysis was confirmed by measuring a standard material 'medium organic content soil' OAS (B2178, BN 217409, with 3.19% ± 0.07 C and 0.27% ± 0.02 N) in triplicate, prepared in the same way as samples with unknown organic carbon contents. TOC deposition rates in periods with and without mass-wasting events were calculated from the derived mass accumulation rates and the measured TOC content at the sediment surface and in layers deposited during mass wasting.

### 2.5. Sediment photographs

Cores A4 and A5 collected from Atacama Trench were vertically split and photographed in a laboratory at the Center for Marine Environmental Sciences, University of Bremen (MARUM) by using a Multi-Sensor Core Logger (MSCL; GEOTEK®) equipped with a line scan camera for high-resolution core image acquisition. These cores were collected in the same multi-corer cast with the cores used for the radionuclide analysis. These photographs are shown in Figure S1.

## 3. Results

### 3.1. Sediment profiles of $^{210}Pb_{ex}$ and TOC in the eutrophic Atacama Trench system

Nine sites were targeted in the Atacama Trench region: Six along the trench axis (A10, A2, A3, A4, A5 and A6), two at abyssal references sites located at each side of the trench (A7 and A9) and one bathyal site located closer to the continent (A1), (Figure 1, Table 1 and Table S2). At five sites, $^{210}Pb_{ex}$ profiles were derived from sediment cores from the same multi-corer cast and analyzed by two different procedures and in two different laboratories (see Materials and Methods for details). Except for slight misalignments of the sediment surface between two cores at A1, A2 and A5, the two approaches provided very similar results and gave confidence in the derived values (Figure 2 and Table 2). As expected, no $^{137}Cs$ was detected in any Atacama Trench sediments due to low $^{137}Cs$ supply in the Southern Hemisphere (Aoyama et al., 2006; Tsurume et al., 2011). At the bathyal site, A1, and the oceanward abyssal site, A7, the $^{210}Pb_{ex}$ profiles presented mono exponential declines from the surface to a sediment depth of approximately 10 cm (Figure 2). However, the concentration of supported $^{210}Pb$ concentration along the upper 9 cm in A1 (0.15-0.18 Bq $g^{-1}$) were clearly higher than the concentrations measured below a 9 cm (0.12-0.14 Bq $g^{-1}$), suggesting that the composition, and thus the source of the sediment might have changed at the time of deposition (Table S2). The TOC contents at these two sites declined gradually with sediment depth, but with much higher values (2.3 % at 0-1 cm depth) at the bathyal site A1 as compared to the abyssal site A7 (0.7 %).

Abyssal site, A9, located close to the edge of the trench, exhibited an apparently disturbed sediment surface with variable $^{210}Pb_{ex}$ concentrations varying between 0.5 and 0.2 $Bq \cdot g^{-1}$ from the sediment surface to 6 cm depth from

here on values declines exponentially (Figure 2). Similarly, the TOC contents within the upper 4 cm appear constant, and thereafter TOC gradually increased with increasing sediment depth (Figure 2). The combined data suggest that the upper disturbed sediment layer was deposited during a mass-wasting event, potentially triggered by two large earthquakes in 2014 which had epicenters near A9 (Table S3).

The hadal site A10, located 30 km west of A9, also showed a similar disturbed sediment profile with constant $^{210}Pb_{ex}$ concentrations along the upper 3 cm, followed by a mono exponential decline down to undetectable levels at 10 cm. The average TOC contents was 1.05 % at 0-3 cm, which is distinctly lower than peak values encountered at 4-5 cm of depth (Figure 2). Abnormal $^{210}Pb_{ex}$ concentrations and TOC contents at 5-12 cm sediment depth at hadal site A2 also suggest the presence of a mass-wasting deposit. The depositional age based on the $^{210}Pb_{ex}$ dating is of about 90 years, coincident with historic earthquakes recorded in the area in 1929 and 1933 (Table S3). $^{210}Pb_{ex}$ and TOC contents at A4 showed an increase at 6-10 cm and 10-14 cm, respectively. These depositional events are possibly linked to the same incident of mass wasting, but the slight misalignment might be related to the fact that profiles originate from two parallel sediment cores. The deposition age of this layer is about 70 years, coinciding with earthquakes in the area that were recorded in 1957 (Table S3). Apart from a few minor excursions, the remaining hadal sites (A3, A5 and A6) all exhibited a steadily decrease in $^{210}Pb_{ex}$ concentration from the surface until reaching background levels in the deeper sediment layers, suggesting no mixing or mass-wasting deposits at these sites during the past 100 years.

Excluding any contributions from mass-wasting deposits, the SR and MAR during steady deposition periods as derived from the $^{210}Pb_{ex}$ concentration profiles amounted to 0.70-0.77 mm $y^{-1}$ (0.037 g $cm^{-2}$ $y^{-1}$) for the bathyal site (A1), 0.33-0.65 mm $y^{-1}$ (0.018-0.024 g $cm^{-2}$ $y^{-1}$) for the oceanward and continental slope abyssal sites (A7 and A9) and 0.29-0.79 mm $y^{-1}$ (0.012-0.093 g $cm^{-2}$ $y^{-1}$) for the hadal sites along the trench axis (Table 2).

**Table 2.** Sedimentation Rate, Mass Accumulation Rate, Core Depth Applied to Calculate the Rates, TOC Content in the Surface (0-1 cm depth) Sediment and Organic Carbon (OC) Deposition rate.

| Trench system | Site | Sedimentation rate (mm $y^{-1}$) | Mass accumulation rate (g $cm^{-2}$ $y^{-1}$) | Depth to calculate the rates (cm) | TOC (%)[a] | OC deposition rate (gC $m^{-2}$ $y^{-1}$) |
|---|---|---|---|---|---|---|
| Atacama | A1 | 0.77 | 0.037 | 0.5-9.5 | 2.32 | 8.58 |
| | | 0.70[b] | 0.037[b] | 0.5-7.5 | | 8.58[b] |
| | A7 | 0.65 | 0.024 | 0.5-9.5 | 0.67 | 1.59 |
| | A9 | 0.33 | 0.018 | 6.5-9.5 | 1.01 | 1.80 |
| | A10 | 0.29 | 0.012 | 2.5-6.5 | 0.94 | 1.16 |
| | A2 | 0.29 | 0.028 | 3.5-5.5 | 0.39 | 1.12 |
| | | 0.49[b] | 0.043[b] | 0.5-4.5 | | 1.67[b] |
| | A3 | 0.79 | 0.093 | 5.5-9.5 | 0.57 | 5.26 |
| | A4 | 0.56 | 0.055 | 0.5-6.5 | 0.58 | 3.15 |
| | | 0.67[b] | 0.062[b] | 0.5-6.5 | | 3.57[b] |
| | A5 | 0.39 | 0.027 | 4.5-9.5 | 0.67 | 1.78 |
| | | 0.48[b] | 0.037[b] | 3.5-9.5 | | 2.13[b] |
| | A6 | 0.43 | 0.032 | 0.5-7.5 | 0.58 | 1.84 |
| | | 0.47[b] | 0.043[b] | 0.5-6.5 | | 2.51[b] |
| Kuril-Kamchatka | KK1 | 0.80 | 0.036 | 0.5-15 | no data | - |
| | KK4 | 0.88 | 0.042 | 9.5-22.5 | no data | - |
| | KK9 | 0.28 | 0.012 | 2.5-7.5 | 1.04 | 1.25 |
| | KK11 | 0.89 | 0.029 | 2.5-4.5 | 1.08 | 3.13 |
| | | 0.49 | 0.053 | 17-23 | 0.92[c] | 4.88 |
| Kermadec | K7 | 0.31 | 0.020 | 0.5-3.5 | 0.37 | 0.73 |
| | K4 | 0.30 | 0.015 | 0.5-3.5 | 0.45 | 0.66 |
| | K6 | 0.39 | 0.029 | 0.5-7.0 | 0.43 | 1.26 |
| Mariana | M1 | - | - | - | 0.49 | - |
| | M2 | 0.39[d] | 0.044[d] | 0.5-6.5 | 0.43 | 1.91 |

*Note.* [a] Averaged value of the two cores in the surface sediments. [b] $^{210}Pb_{ex}$ was measured at ECU. [c] Averaged value of the upper mass wasting event layer. [d] Glud et al. (2013)

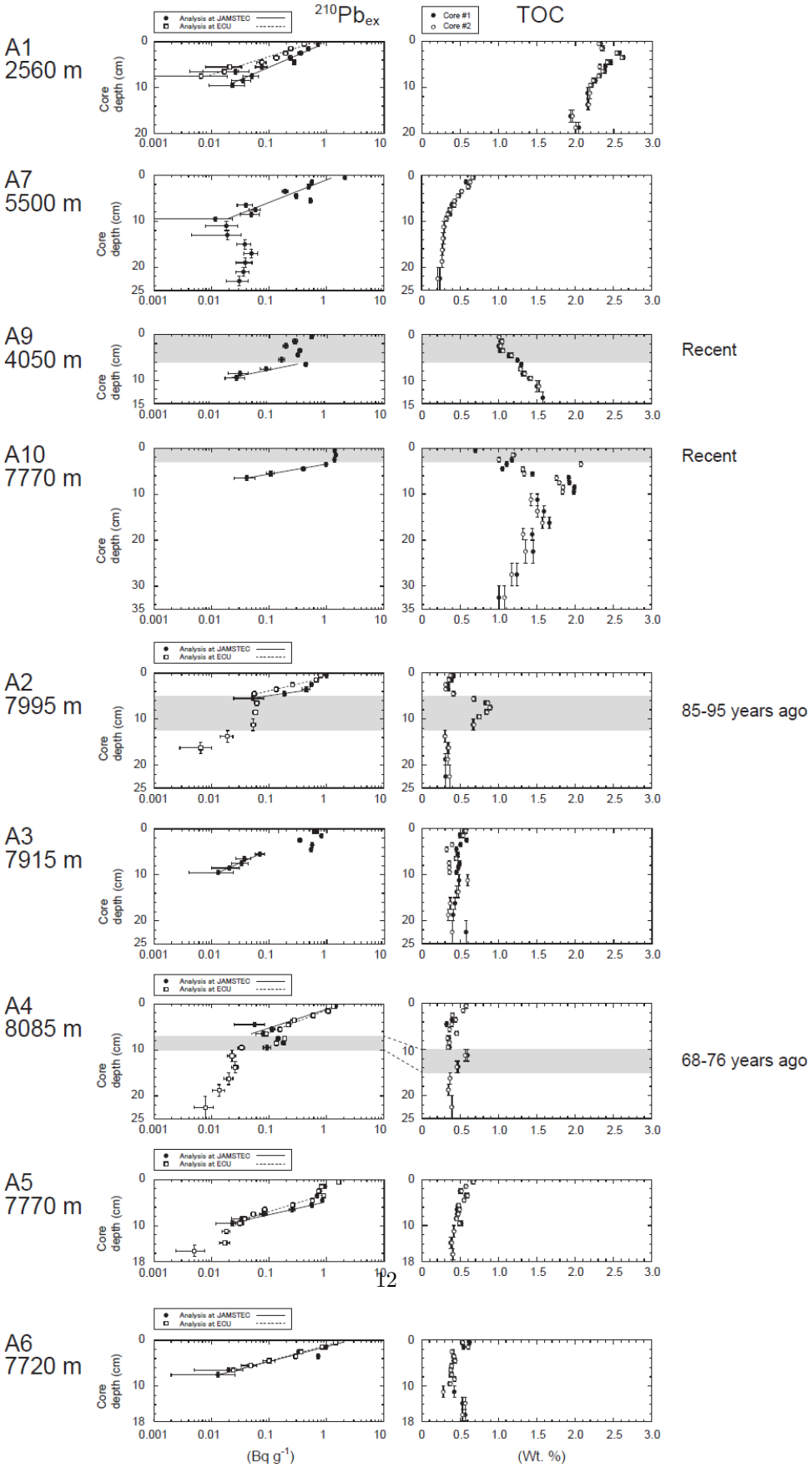
$^{210}Pb_{ex}$
TOC
Analysis at JAMSTEC
Analysis at ECU
Core #1
Core #2
A1
2560 m
A7
5500 m
A9
4050 m
Recent
A10
7770 m
Recent
A2
7995 m
85-95 years ago
A3
7915 m
A4
8085 m
68-76 years ago
A5
7770 m
A6
7720 m
Core depth (cm)
(Bq g$^{-1}$)
(Wt. %)

**Figure 2.** $^{210}Pb_{ex}$ and TOC profiles measured in sediment cores recovered in the Atacama Trench region. Sediment layers deposited during mass wasting events, as inferred from elevated and constant $^{210}Pb_{ex}$ activities over distinct depth intervals and abnormal TOC distribution are shown in gray hatches. Solid and dashed lines in the $^{210}Pb_{ex}$ graphs were obtained by exponential curve fitting from the corresponding $^{210}Pb_{ex}$ plots.

### 3.2. Sediment profiles of $^{210}Pb_{ex}$, $^{137}Cs$ and TOC in the eutrophic Kuril-Kamchatka Trench system

Four hadal sites were targeted in the Kuril-Kamchatka Trench system (Figures 1a and 3a). As for the Atacama Trench, some sites had sediment horizons with constant $^{210}Pb_{ex}$ that reflect rapid deposition by mass wasting. This pattern was clear at KK4 where two layers with distinct signatures representative of mass wasting were identified at 0-10 cm and 23-40 cm, respectively (Figure 3a). The surface layer is likely related to a large earthquake that occurred close to site KK4 in 2006, while the deeper layer is related to an unidentified mass-wasting event more than 100 years old (Table S3). In contrast, the sediment at KK11 reflected a single mass-wasting event surrounded by two periods of low, constant sedimentation rates (Figure 3a and Table 2). The time for the mass wasting coincides with two significant earthquakes in the region in 1995 and 1996. Unlike sediments from the Atacama Trench, $^{137}Cs$ was detected at all Kuril-Kamchatka sites. At KK4 and KK11, $^{137}Cs$ extended into the layers below the mass -wasting deposits, confirming that these layers were deposited after 1956, when $^{137}Cs$ fallout was intensified by atmospheric nuclear tests (Hirose et al., 2008). The $^{210}Pb_{ex}$ profiles at KK1 and KK9 showed no distinct signatures of deposits from mass wasting (Figure 3a). Excluding the sediment contribution from mass-wasting events, the derived SR and MAR at the four hadal sites in Kuril-Kamchatka Trench were 0.80 mm $y^{-1}$ (0.036 g $cm^{-2}$ $y^{-1}$) at KK1, 0.88 mm $y^{-1}$ (0.042 g $cm^{-2}$ $y^{-1}$) at KK4, 0.28 mm $y^{-1}$ (0.012 g $cm^{-2}$ $y^{-1}$) at KK9 and 0.89 mm $y^{-1}$ (0.028 g $cm^{-2}$ $y^{-1}$) at KK11 (Table 2). The TOC content at both KK9 and KK11 gradually decreased from the surface to the maximum measuring depth. Unfortunately, no TOC data are available from KK1 and KK4.

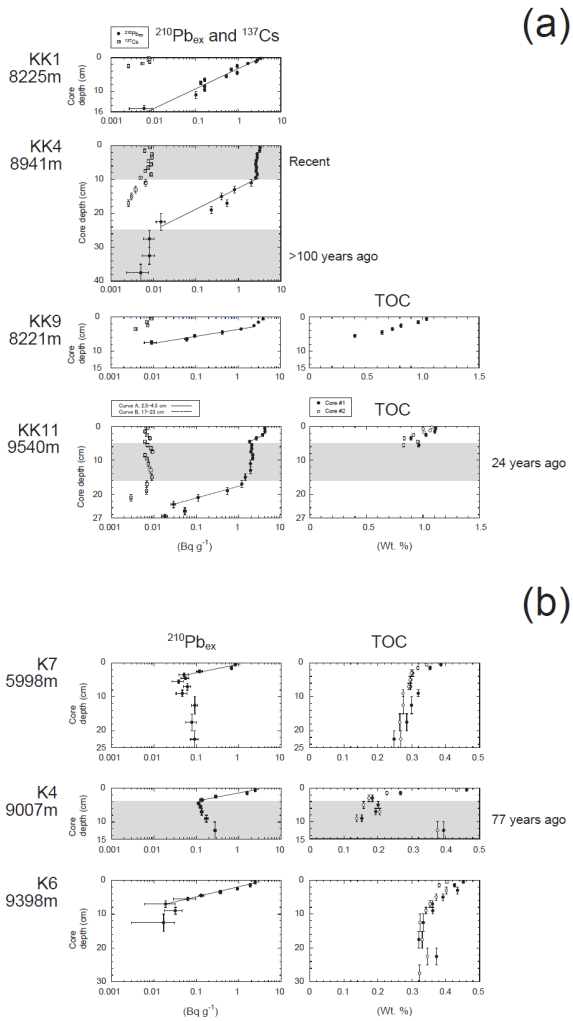
(a)
$^{210}Pb_{ex}$ and $^{137}Cs$
KK1
8225m
KK4
8941m
Recent
>100 years ago
TOC
KK9
8221m
TOC
KK11
9540m
24 years ago
Core depth (cm)
(Bq g$^{-1}$)
(Wt. %)
(b)
$^{210}Pb_{ex}$
TOC
K7
5998m
K4
9007m
77 years ago
K6
9398m

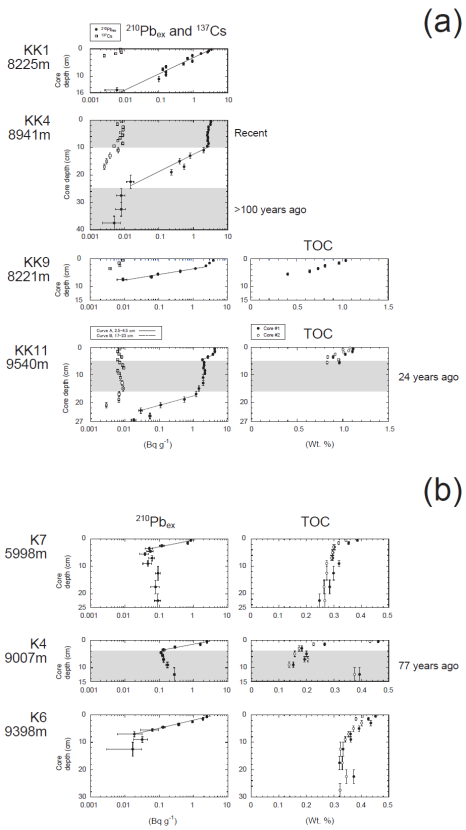


**Figure 3.** $^{210}$Pb$_{ex}$, $^{137}$Cs and TOC profiles measured in sediment cores in the Kuril-Kamchatka (a) and the Kermadec Trench (b) regions. Sediment layers deposited during mass wasting events, as inferred from elevated and constant $^{210}$Pb$_{ex}$ activities over distinct depth intervals (for both trench cores) and abnormal TOC distribution (for Kermadec Trench cores only) are shown in gray hatches. Solid lines in the $^{210}$Pb$_{ex}$ graphs were obtained by exponential curve fitting from the corresponding $^{210}$Pb$_{ex}$ plots.

### 3.3. Sediment profiles of $^{210}$Pb$_{ex}$ and TOC in the mesotrophic Kermadec Trench.

Three sites were sampled in the Kermadec Trench: one at a nearby abyssal reference site (K7) and two located in the trench axis (K4 and K6). The $^{210}$Pb$_{ex}$ concentration profiles at K7 and K6 showed a steep decrease from the surface to a depth of 4 and 8 cm respectively, before reaching a stable low level to the bottom of the core (25 and 30 cm, respectively; Figure 3b). The $^{210}$Pb$_{ex}$ concentration profile of K4 showed enhanced $^{210}$Pb$_{ex}$ concentrations towards the bottom of the cores which coincided with an elevated TOC content, instead of the gradual decrease seen at K7 and K6 cores (Figure 3b). This layer is possibly formed by mass wasting from the upper trench slope located west of the trench

axis (Ballance et al., 2000). Based on the sedimentation rate derived from the $^{210}Pb_{ex}$ concentrations, the deposition of this layer would have occurred before 1940, which is compatible with two major earthquakes that occurred in the region in 1917 and 1919 (Table S3). Like the Atacama Trench, no $^{137}Cs$ was detected in any of the sampled Kermadec Trench sediments. The derived SR and MAR rates at the abyssal reference site (K7) amounted to 0.31 mm $y^{-1}$ (0.020 g $cm^{-2}$ $y^{-1}$) while values at the two hadal sites were 0.30-0.39 mm $y^{-1}$ (0.015-0.029 g $cm^{-2}$ $y^{-1}$), ignoring any contributions from mass wasting (Table 2).

1. **Sediment profiles of $^{210}Pb_{ex}$, $^{137}Cs$, and TOC in the oligotrophic Mariana Trench**

Two sediment cores from the Mariana Trench region were investigated: one from an abyssal reference site (M1) and one from the trench axis (M2). The $^{210}Pb_{ex}$ concentration and the TOC content has previously been presented in Glud et al. (2013). The $^{210}Pb_{ex}$ concentrations at the abyssal site were elevated at the surface, but values remained relatively low and without any distinct decline with increasing sediment depth (Figure 4). It was not possible to derive any SR and MAR from the data at site M1. The recovered sediment cores contained many manganese nodules and previous investigations have observed high levels of manganese oxide in subsurface sediments from this region (Iijima et al., 2016), and therefore the observed $^{210}Pb_{ex}$ profile at this site maybe strongly confounded by the release of $^{222}Rn$ from manganese oxide (DeMaster & Cochran, 1982).

The profile of $^{210}Pb_{ex}$ at the hadal site M2 showed a steep exponential decline from the surface down to 8 cm depth, overlying a sector of relatively low stable $^{210}Pb_{ex}$ concentrations down to 25 cm. The $^{137}Cs$ signal was detected from the surface to 6 cm depth. The sedimentation and mass accumulation rates derived from the $^{210}Pb_{ex}$ profile amounted to 0.39 mm $y^{-1}$ (0.044 g $cm^{-2}$ $y^{-1}$) (Table 2). The $^{210}Pb_{ex}$ profiles suggest that the sediment below 8 cm depth was formed by a past unidentified mass-wasting event, which occurred at least 100 years ago. The downcore TOC content was highly irregular but averaged 0.37 % without any distinct depth pattern.

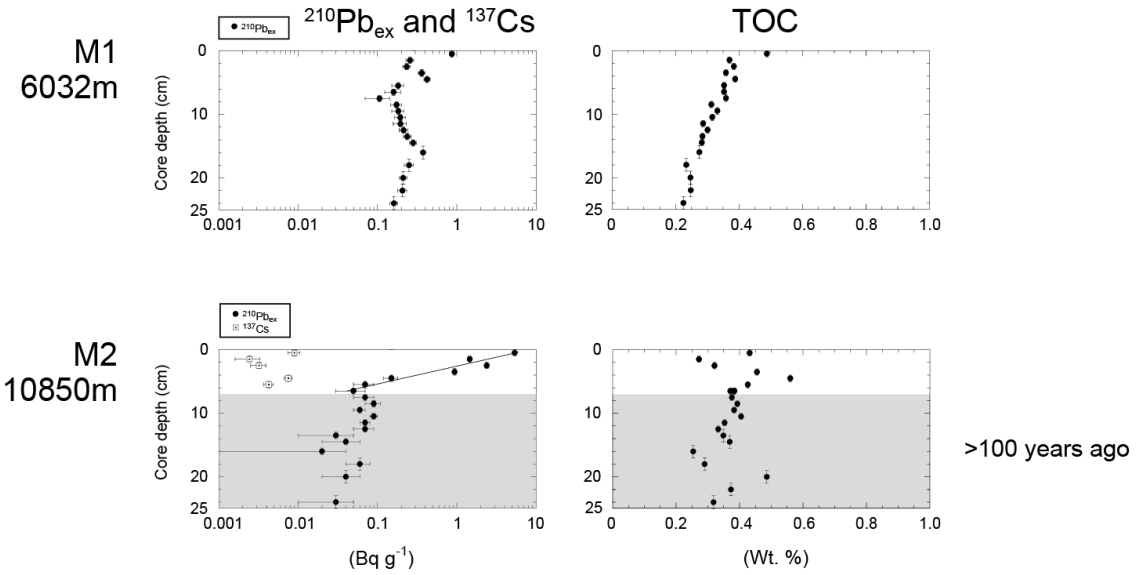


**Figure 4.** $^{210}Pb_{ex}$, $^{137}Cs$ and TOC profiles measured in sediment cores in the Mariana Trench region. Sediment layers deposited during mass wasting events, as inferred from constant $^{210}Pb_{ex}$ activities and TOC distribution are shown in gray hatches. Solid lines in the $^{210}Pb_{ex}$ graphs were obtained by exponential curve fitting from the corresponding $^{210}Pb_{ex}$ plots.

1. **Discussion**

### 4.1. Sedimentation, focusing and mass accumulation along trench axes.

This study uses $^{210}Pb_{ex}$ and TOC profiles to estimate SR, MAR and carbon deposition rates in some of the deepest trenches on Earth. Sediment layers with constant and/or elevated concentrations of $^{210}Pb_{ex}$ and unusual excursions in the TOC contents, were interpreted as deposits formed during mass-wasting events. It is well established that high densities of infauna, as found in coastal margins or along continental slopes, can strongly affect sediment through bioturbation, resulting in high, constant $^{210}Pb_{ex}$ concentrations at the sediment surface (Nozaki et al., 1977; McKee et al., 1983; DeMaster et al., 1985). SR and MAR in such settings are usually derived by ignoring values from the mixed surface layer and only use the mono-exponential decline of $^{210}Pb_{ex}$ in the underlying, non-bioturbated sediments layers (Nozaki et al., 1977; Nittrouer et al., 1984; Glud el al., 1998). We cannot exclude that bioturbation may have affected the distribution of $^{210}Pb_{ex}$ in surface sediments from some of our targeted sites indicating constant $^{210}Pb_{ex}$ concentrations (i.e., A3, A5 and KK4). However, a sub-set of hadal sediment cores were imaged and exhibited undisturbed lamination (Figure S1) suggesting little or no bioturbation. While the sediments would undoubtedly host small-bodied infauna; meiofauna; (e.g., Leduc & Row-

den, 2018), no larger bioturbating macrofauna were found in any cores during sectioning. Hadal sediments host negligible amounts of bioturbating macrofauna, as compared to shallow water environments (Brandt et al., 2018). In a few instances, surface sediment exhibited fluctuating $^{210}Pb_{ex}$ concentrations with constant persistent TOC contents (i.e., A3 and A5), which could be related to shaking induced by seismic activity as recorded by time-series in situ photographs at sediment surface in bathyal continental slope, Sanriku region, Japan (Oguri et al., 2016) and in sedimentary structures at seismic active settings at the continental slope of the Japan Trench (Ikehara et al., 2021). We therefore argue that layers of relatively constant, elevated $^{210}Pb_{ex}$ concentrations in hadal sediments reflect mass-wasting and/or seismic events rather than intense sediment mixing by infauna.

To quantitatively assess the potential enhancement of material focusing along the trench axes we derived the focusing factors in the four investigated trench regions. We quantified the focusing factors at the four abyssal sites adjacent to the respective trenches were similar, ranging from 1.17 (A9) to 2.05 (A7) and with an average of 1.67 ± 0.32 (Table 3). These values indicate that some material focusing exists along the trench edge, although it might also partly reflect that the pelagic deficient $^{210}Pb$ inventory were derived from data obtained at some distance from the respective trench regions (Table S1). We cannot exclude that these sites might have different deficient $^{210}Pb$ inventories than waters above the actual trench region caused by intensified $^{210}Pb$scavenging along the trench boundaries (e.g., Nozaki et al., 1997). Regardless, the vertical focusing factors along the hadal trench axes were derived by applying the same pelagic data and generally expressed elevated values, ranging from 1.06 (A10) to 3.54 (K6) and with an average of 2.12 ± 0.66 (Table 3). The generally elevated focusing factors along the hadal trench axes suggest downslope material transport towards the trench interior even during periods with no significant mass wasting (Figure 5a). The few hadal sites with relatively low focusing factors (i.e., 1.06 at A10 and 1.24-1.81 at A2; Table 3) could potentially imply limited focusing or winnowing driven by hydrography interacting with local bathymetric structures (Turnewitsch et al., 2014).

**Table 3.** $^{210}Pb_{ex}$ Inventories in Abyssal and Hadal Sediments, $^{226}Ra$, $^{210}Pb$ and Deficient $^{210}Pb_{ex}$ Inventories in the Water Column and Focusing Factor.

| Trench system | Site | Water depth (m) | $^{210}Pb_{ex}$ inventory in sediment no or excluding mass wasting layer (Bq cm$^{-2}$) | | $^{210}Pb_{ex}$ inventory in sediment including mass wasting layer (Bq cm$^{-2}$) | | $^{226}Ra$ inventory in the water column (Bq cm$^{-2}$) | $^{210}Pb$ inventory in the water column (Bq cm$^{-2}$) | Deficient $^{210}Pb_{ex}$ inventory in the water column (Bq cm$^{-2}$) | | Focusing factor no or excluding mass wasting layer | | Focusing factor including mass wasting layer | |
|---|---|---|---|---|---|---|---|---|---|---|---|---|---|---|
| Atacama | A7 | 5500 | 1.25 | (0.11) | | | 2.19 | 1.58 | 0.61 | | 2.05 | (0.15) | | |
| | A9 | 4050 | 0.29 | (0.04) | 0.98 | (0.09) | 1.42 | 1.17 | 0.25 | | 1.17 | (0.16) | 3.98 | (0.35) |
| | A10 | 7770 | 1.27 | (0.08) | 2.16 | (0.09) | 3.41 | 2.22 | 1.20 | | 1.06 | (0.07) | 1.81 | (0.08) |
| | A2 | 7995 | 2.28 | (0.23) | 2.85 | (0.34) | 3.53 | 2.28 | 1.26 | | 1.81 | (0.19) | | |
| | | | 1.56[a] | (0.09) | 1.66[a] | (0.11) | | | | | 1.24 | (0.07) | 1.32 | (0.09) |
| | A3 | 7915 | 2.37 | (0.15) | | | 3.49 | 2.26 | 1.23 | | 1.92 | (0.14) | | |
| | A4 | 8085 | 2.17 | (0.12) | 2.50 | (0.15) | 3.58 | 2.30 | 1.28 | | 1.70 | (0.09) | 1.96 | (0.12) |
| | | | 2.73[a] | (0.19) | 2.97[a] | (0.21) | | | | | 2.13 | (0.16) | 2.32 | (0.16) |
| | A5 | 7770 | 3.24 | (0.15) | | | 3.41 | 2.22 | 1.20 | | 2.71 | (0.14) | | |
| | | | 3.22[a] | (0.20) | | | | | | | 2.69 | (0.16) | | |
| | A6 | 7720 | 2.47 | (0.14) | | | 3.39 | 2.20 | 1.18 | | 2.09 | (0.12) | | |
| | | | 2.44[a] | (0.14) | | | | | | | 2.06 | (0.12) | | |
| Kuril-Kamchatka | KK1 | 8225 | 3.00 | (0.07) | | | 4.00 | 2.26 | 1.74 | | 1.72 | (0.01) | | |
| | KK4 | 8941 | 3.35 | (0.07) | 11.3 | (0.05) | 4.37 | 2.45 | 1.92 | | 1.75 | (0.02) | 5.89 | (0.03) |
| | KK9 | 8221 | 3.14 | (0.03) | | | 4.00 | 2.26 | 1.74 | | 1.81 | (0.02) | | |
| | KK11 | 9540 | 6.84 | (0.15) | 14.2 | (0.06) | 4.69 | 2.62 | 2.07 | | 3.31 | (0.02) | 6.87 | (0.03) |
| Kermadec | K7 | 6080 | 1.04 | (0.08) | | | 2.26 | 1.52 | 0.74 | | 1.42 | (0.11) | | |
| | K4 | 9300 | 2.30 | (0.06) | 2.32 | (0.05) | 3.44 | 2.19 | 1.25 | | 1.84 | (0.05) | 1.86 | (0.04) |
| | K6 | 9555 | 4.66 | (0.18) | | | 3.59 | 2.28 | 1.31 | | 3.54 | (0.14) | | |
| Mariana | M1 | 6032 | 1.79[b] | (0.09) | – | | | | 1.15[c] | (0.43) | 1.56[c] | (0.59) | | |
| | M2 | 10850 | 4.80 | (0.91) | 5.05[b] | (0.80) | | | 2.64[c] | (0.80) | 1.82 | (0.67) | 1.91[c] | (1.6) |

*Note.* [a] $^{210}Pb_{ex}$ was measured at ECU, [b] Depth integration to 25 cm (Glud et al. 2013; Turnewitsch et al. 2014), and [c] Turnewitsch et al. (2014).

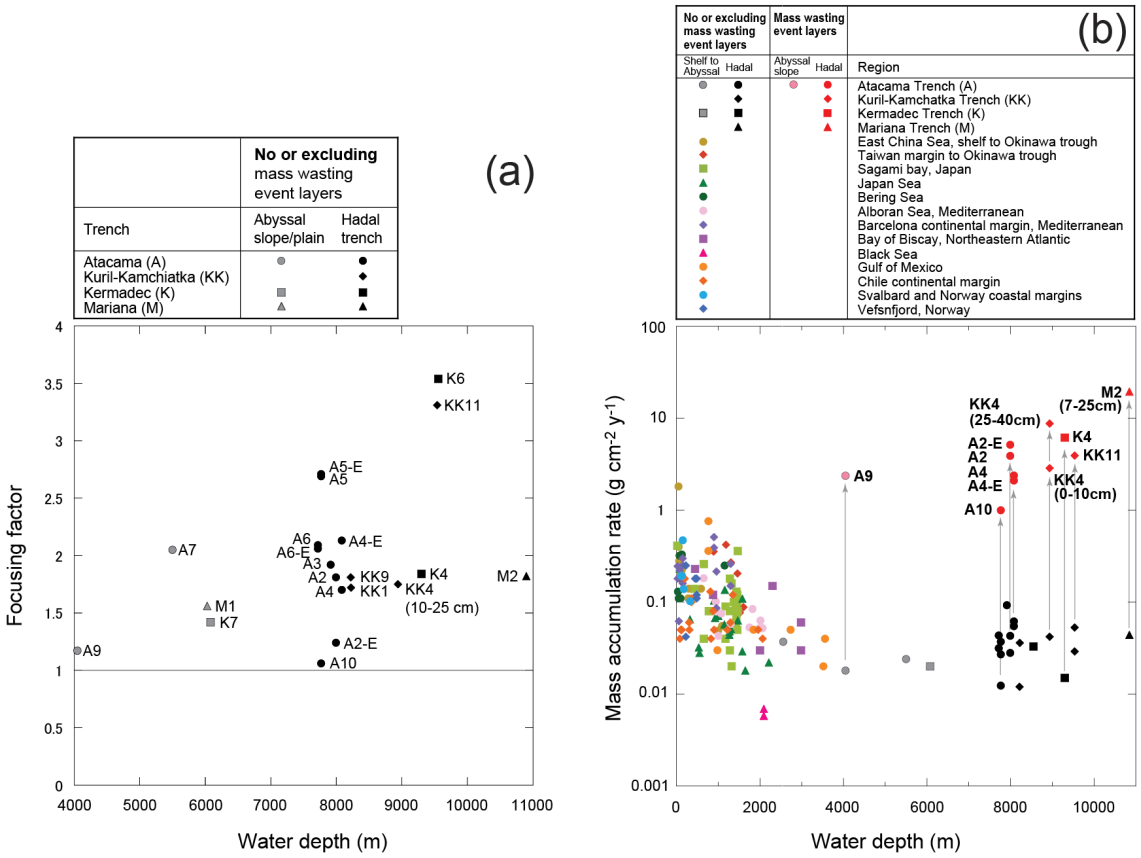


**Figure 5.** (a) The derived focusing factor for the targeted sites ignoring sedimentary depositions mediated by mass wasting events as identified by profiles of $^{210}Pb_{ex}$ and TOC distribution. (b) Mass accumulation rates as a function of water for the compiled data include studies from: East China Sea shelf to Okinawa trough (Oguri et al., 2003), Taiwan margin to Okinawa trough (Chung & Chang, 1995), Sagami Bay (Kato et al., 2003), Japan Sea (Hong et al., 1997), Bering Sea (Oguri et al., 2012), Alboran Sea (Masqué et al., 2003), Barcelona continental margin (Sanchez-Cabeza et al., 1998), Bay of Biscay (Radakovitch & Heussner, 1999), Black Sea (Crusius & Anderson, 1992; Buesseler & Benitez, 1994), Gulf of Mexico (Yeager et al., 2004), Chile continental margin (Muñoz et al., 2004), Svalbard and Norway coastal margins (Glud et al., 1998), Vefsnfjord (Heldal et al., 2021) and the current study. The abbreviation indicate the respective trenches and the specific sites in the respective trenches as outlined in Table 1. Suffix -E after A in the plots represents that the $^{210}Pb_{ex}$ concentrations was measured at Edith Cowan University. The others without suffix were measured at Japan Agency for Marine-Earth Science and Technology (A, K and M) and the Scottish Universities Environmental Research Centre (KK), respectively.

The derived SR and MAR for the investigated hadal sites are relatively high, even when sediment layers deposited during mass wasting are excluded from the calculation and compare to the MAR estimated for many continental slopes (Figure 5b), and generally exceed values from abyssal settings (Figure 5b, and Table 2). These findings suggest considerable material focusing along trench axes that is presumably mediated by gravity driven, near-bed, downslope material transport that is potentially modulated by tidal-driven internal seiche (Turnewitsch et al., 2014; Van Haren et al., 2020). Seven hadal sites had distinct records of mass wasting (A4, A9, A10, KK4, KK11, K4 and M2), and inclusion of $^{210}Pb_{ex}$ inventories from these deposits markedly increased the MAR by almost 2 orders of magnitude (Table 3 and Figure 5b). Site A9, at the continental edge of the Atacama Trench, was only 4050 m deep, but was clearly affected by a mass-wasting event that also was reflected at the nearby hadal site at 7770 m depth (A10). This pattern suggests that the steeper slope angles encountered between the continental margin and trench axis may facilitate significant translocation of material from relatively shallow settings to the hadal trench axis. The importance of mass wasting for the redeposition of material in hadal trenches has been demonstrated previously (Itou et al., 2000; Bao et al., 2018), but here we document that mass-wasting events during the past 100 years have been responsible for at least 34 times enhancement of the deposition along the investigated trench axes (Figure 5b).

Our data from four different trenches systems show that mass wasting might place hadal trench sites among the marine habitats with the highest mass accumulation rates (Figure 5b). Additionally, our assessments also suggest that trenches are characterized by continuous accumulation of material focusing, even during periods without significant mass wasting. Both the continuous and the erratic enhancement of material deposition might have important implications for the balance between microbial mineralization and burial of organic material and thereby long-term carbon sequestration in trench regions and the deep sea in general.

### 4.2. Deposition of organic carbon in hadal trenches.

Hadal trench sediments exhibit 2-5 times higher microbial mineralization rates compared to adjacent abyssal sediments (Glud et al., 2013; Wenzhöfer et al., 2016; Luo et al., 2019) and benthic hadal mineralization rates generally correlate well to net primary productivity in the surface ocean (Glud et al., 2021). The four targeted trench regions underly surface waters of very different net primary productivity (Table 1; from 50.4 to 449 gC $m^{-2}$ $y^{-1}$), but there was no apparent relationship between MAR or organic carbon deposition rate and the net primary productivity at the surface ocean (Tables 1 and 2). The disposition and accumulation rates of organic carbon exhibited extensive site specific variations variability was large (Figure 5 and S2). These observations suggest that deposition dynamics is strongly modulated by local bathymetry but highly enhanced during mass wasting events Generally, the variability in organic carbon deposition rates is mainly caused by differences in SR and MAR rather

than the TOC content (Table 2). For instance, the variation in SR and MAR along the Atacama Trench range by more than 7 fold (0.012-0.093 g $cm^{-2}$ $y^{-1}$), while the variation in TOC content is less than 3 fold (0.39-1.01 %) (Table 2). The variability imposed by the highly complex bathymetry and corresponding geomorphology of subducting trenches (e.g., Stewart & Jamieson, 2018) underpin the challenge of extrapolating single point measurements to an entire trench system, let alone to hadal trenches in general. Inclusion of contributions from local, unpredictable mass-wasting events clearly further enhance the encountered variations of MAR and organic carbon deposition rates along the trench axis (Table 2, Figures 5 and 6). The high spatiotemporal variations in deposition of material likely play a central role in the distribution and dynamics of biological communities in trenches and thus the relative accumulation of organic material in the hadal sediments.

### 4.3. Accumulation of organic carbon in hadal trenches.

Burial or retention of organic carbon in marine sediments are generally correlated with MAR (Canfield, 1994). In regions with low MAR, most of the deposited organic material is efficiently mineralized by aerobic microbial respiration. However, increasing deposition of organic carbon intensifies microbial mineralization and reduces the benthic $O_2$ availability whereby carbon mineralization to a larger extent is mediated by less efficient anaerobic mineralization. This process generally leads to relatively higher organic carbon accumulation at such settings (Burdige, 2007). To estimate the relative accumulation of deposited organic material, we combined the derived TOC deposition rates ($D_R$) with previously published measurements of benthic mineralization rate ($M_R$) as derived from benthic $O_2$ consumption rates for the three trench systems where such measurements are available (Glud et al., 2013 & 2021). To covert the benthic $O_2$ consumption rates to organic carbon mineralization rates we assumed a Respiratory Quotient (RQ) for the benthic mineralization of 0.85. The relative accumulation of organic carbon ($R_{OM}$) in the sediment record without accounting for mass wasting should equal:

$$R_{\mathrm{OM}} = \frac{D_R}{D_R + M_R} \bullet 100\ (\%)\ (3)$$

The hadal values ranged from 16 % (A10) to 77 % (M2) with an overall average of 40±16 %, which compare to values from many coastal margins and shelf systems (Figure 6). This implies that even without mass wasting, hadal sediments appear to be quantitatively important sites for carbon sequestration in the deep sea. The inclusion of deposits from mass wasting, makes this proposition even more explicit. Four of the targeted sites were affected by mass wasting and including deposition during these events enhanced the deposition of organic carbon 21-365 times and accumulation of the organic carbon reached values between 93-99 % (Table 4 and Figure 6). These assessments demonstrate that despite highly elevated microbial mineralization, hadal regions accumulate relatively large amounts of organic material. The current findings align with other recent investigations from the Japan Trench that demonstrated the importance

of tectonic induced mass wasting for translocating organic carbon to the hadal environment (Bao et al., 2018; Kioka et al., 2019b) and previous indirect evidence arguing for high carbon accumulation in hadal sediments (Luo et al., 2017; Xu et al., 2021) and with recent findings of highly elevated sequestration of black carbon in some hadal settings (Zhang et al. 2022).

**Table 4**.

Depth of Mass-Wasting Event Layer, Amount of Organic Carbon (OC) Deposition Per Event, OC Deposition Rate without Mass-Wasting Event and OC Depositional Ratio with/without Mass-Wasting Events of the Hadal Sediments.

| Trench sytem | Site | Depth of mass-wasting event layer (cm) | Amount of OC preserved per single mass-wasting event (gC $m^{-2}$) | OC deposition rate without mass-wasting event (gC $m^{-2}$ $y^{-1}$) | OC deposition ratio with/without mass-wasting event |
|---|---|---|---|---|---|
| Atacama | A10 | 0-3 | 105 | 1.16 | 91 |
| | A2 | 5-12 | 295-388 | 1.12-1.67 | 177-346 |
| | A4 | 7-10 | 75-85 | 3.15-3.57 | 21-27 |
| Kermadec | K4 | 4-15 | 181 | 0.66 | 276 |
| Mariana | M2 | 7-25 | 697 | 1.91 | 365 |

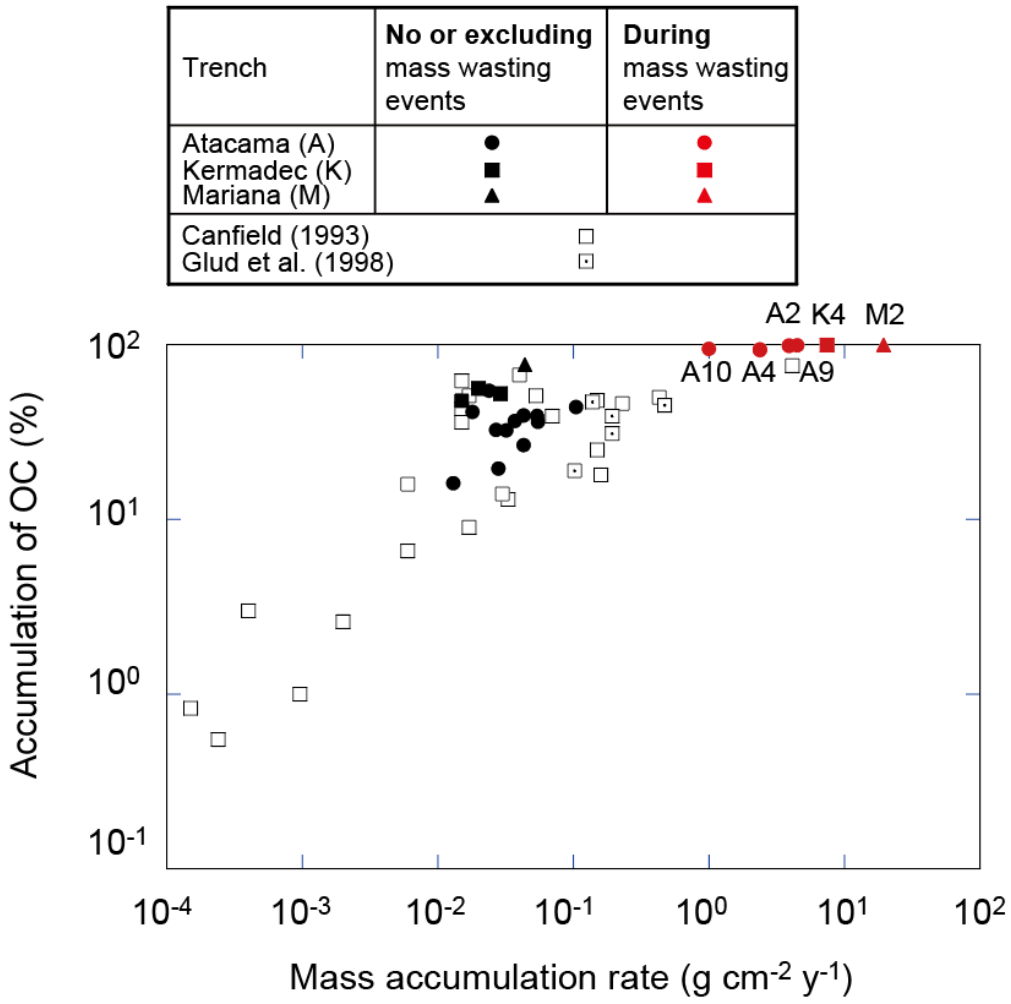


**Figure 6.** The accumulation of organic carbon versus as derived from deposition and mineralization rates versus the mass accumulation rates quantified form a range of marine settings. The hadal data of the current study are plotted along with previous values collected at a depth range from 10 m to 5330 m presented in Canfield (1993) and Glud et al. (1998). The abbreviation indicate the respective trenches and the specific sites in the respective trenches as outlined in Table 1.

## 1. Conclusions and Perspectives

The current investigation demonstrates that for the past ~100 years SR and MAR and organic carbon deposition in four hadal trenches systems exceed values from the adjacent abyssal settings. The enhanced material transport is mediated by downslope focusing but mainly by mass wasting, although the vari-

ations both within and between individual trenches is considerable due to local bathymetry, and spatiotemporal dynamics as induced by mass wasting events. However, the sources and characteristics of the material reaching the trench axes are still poorly resolved (Luo et al., 2019; Lin et al., 2021; Xu et al., 2021). While the deposited organic material sustains high biological activity (Glud et al. 2021), it apparently also leads to considerable sequestration of organic material along the trench axes. During periods without mass wasting, the burial efficiency along the trench axes are within the same range as values encountered at oceanic margins or along continental slopes, but mass wasting markedly enhance hadal accumulation of organic material. The efficiency of anaerobic microbial degradation in subsurface sediments enriched in organic material remain unknown and thus the timescale of hadal carbon retention require further insights on anaerobic mineralization at hadal depth. The study adds to the growing evidence that hadal trenches are complex (Stewart & Jamieson, 2018) and dynamic habitats, and that site-specific conditions challenge areal extrapolations even within a given trench system let alone across different trench systems.

**Acknowledgements**

We great fully acknowledge the captains and the crews of R/V Sonne (SO250 and SO261), R/V Tangaroa (TAN1711) and R/V Yokosuka (YK10-11). Pei-Chuan Chuang, Emmanuel Okuma (University of Bremen), Axel Nordhausen, Volker Asendorf (Max Planck Institute for Marine Microbiology), Anni Glud, Clemens Schauberger and Morten Larsen (University of Southern Denmark) are thanked for onboard assistance. Jiřina Stehlíková and Robert Turnewitsch (Scottish Association for Marine Science) are thanked for sediment sampling in the Kuril-Kamchatka Trench. Sunaho Kubo (Japan Agency for Marine-Earth Science and Technology) is thanked for the preparation of sediment samples from Atacama and Kermadec. We are also grateful to help by the lander team of the YK10-11 cruise (Nippon Marine Enterprise, Co. LTD.). This study is supported by: The ERC Advanced grant "Benthic diagenesis and microbiology of hadal trenches" grant number 669947, the JSPS Grants-in-Aid for Scientific Research grant number JP20H02013, The Coasts & Oceans Centre of New Zealand's National Institute of Water & Atmospheric Research, The Max Planck Society, JAMSTEC and the Danish National Research Foundation through HADAL, grant number DNRF145. Funding was provided to PM through an Australian Research Council LIEF Project (LE170100219). This work is contributing to the ICTA ''Unit of Excellence'' (MinECo, MDM2015-0552). The IAEA is grateful for the support provided to its Environment Laboratories by the Government of the Principality of Monaco. HAS publishes with the permission of the Executive Director of the British Geological Survey (United Kingdom Research and Innovation).

**Data availability statement**

The data set for this study are available at https://drive.google.com/drive/folders/1Yf-UyNPhlG5iyhvQ8UNI_6f73Fa804dW?usp=sharing

## Supporting information

This supporting information contains two figures (Figures S1 and S2) and three tables (Table S1 to S3).

## References


Aoyama, M., Hirose, K. & Igarashi, Y. (2006). Re-construction and updating our understanding on the global weapons tests $^{137}$Cs fallout. *Journal of Environmental Monitoring*, *8*(4), 431–438. https://doi.org/10.1039/B512601K

Arai, K., Naruse, H., Miura, R., Kawamura, K., Hino, R., Ito, Y., Inazu, D., Yokokawa, M., Izumi, N., Murayama, M., Kasaya, T. (2013). Tsunami-generated turbidity current of the 2011 Tohoku-Oki earthquake. *Geology*, *41*(11), 1195–1198. https://doi.org/10.1130/G34777.1

Ballance, P. F., Follas, H. A., Forggatt, P. C. & Mikhailic, E. V. (2000). Continent-derived vitric mud and mafic-arc rocks in deep Kermadec Trench diamictons. *Journal of Sedimentary Research*, *70*(1), 140–150. https://doi.org/10.1306/2DC40905-0E47-11D7-8643000102C1865D

Bao, R., Strasser, M., McNichol, A. P., Haghipour, N., McIntyre, C., Wefer, G. & Eglinton T. I. (2018). Tectonically-triggered sediment and carbon export to the hadal zone. *Nature Communications*, *9*, 121(2018), https://doi.org/10.1038/s41467-017-02504-1

Barnett P. R. O., Watson, J. & Connelly, D. (1984). A multiple corer for taking virtually undisturbed samples from shelf, bathyal and abyssal sediments. *Oceanologica Acta*, *7*(4), 399–408. https://doi.org/10.1017/S0269727000014846

Behrenfeld, M. J., Paul G. & Falkowski, P. G. (1997). Photosynthetic rates derived from satellite-based chlorophyll concentration. *Limnology and Oceanography*, 42, 1–20. https://doi.org/10.4319/lo.1997.42.1.0001

Berger, W. H., Fisher, K., Lai, G. & Wu, G. (1987). Ocean carbon flux: global maps of primary production and export production. C. Agegian (Ed.), *Biogeochemical cycling and fluxes between the deep euphotic zone and other oceanic realms, Research Report 88–1, NOAA National Undersea Research Program (1987)*, pp. 131–176.

Brandt, A., Frutos, I., Bober, S., Brix, S., Brenke, N., Guggolz, T. et al. (2018). Composition of abyssal macrofauna along the Vema Fracture Zone and the hadal Puerto Rico Trench, northern tropical Atlantic. *Deep Sea Research Part II: Topical Studies in Oceanography*, *148*, 35–44. https://doi.org/10.1016/j.dsr2.2017.07.014

Brandt, A., Brix, S., Riehl, T. & Malyutina, M. (2020). Biodiversity and biogeography of the abyssal and hadal Kuril-Kamchatka trench and adjacent NW Pacific deep-sea regions. *Progress in Oceanography*, *181*, (2020)102232. https://doi.org/10.1016/j.pocean.2019.102232

Buesseler K.O. & Benitez, C. R. (1994). Determination of mass accumulation rate and sediment radionuclide inventories in the deep Black Sea. *Deep Sea Research Part I: Oceanographic Research Papers*, *41*(11–12), 1605–1615. https://doi.org/10.1016/0967-0637(94)90064-7

Burdige, D. J. (2007). Preservation of organic matter in marine sediments: controls, mechanisms, and an imbalance in sediment organic carbon budgets. *Chemical Reviews*, *107*(2), 467–485. https://doi.org/10.1021/cr050347q

Canfield, D. E. (1993). Organic matter oxidation in marine sediments. In Wollast, R., Mackenzie, F.T & Chou, L. (Eds.) *Interactions of C, N, P and S biogeochemical cycles and global change, 4. NATO ASI Series I: Global Environmental Change* (pp. 332–363). Springer-Verlag, Berlin Heidelberg: NATO Scientific Affairs Division. https://doi.org/10.1007/978-3-642-76064-8

Canfield, D. E. (1994). Factors influencing organic carbon preservation in marine sediments. *Chemical Geology*, *114*(3–4), 315–329. https://doi.org/10.1016/0009-2541(94)90061-2

Chung, Y. & Chang, W. C. (1995). Pb-210 fluxes and sedimentation rates on the lower continental slope between Taiwan and the South Okinawa Trough. *Continental Shelf Research*, *15*(2–3), 149–164.

Chung, Y. & Craig, H. (1973). Radium-226 in eastern equatorial pacific. *Earth and Planetary Science Letters, 17*(2), 306–318. https://doi.org/10.1016/0012-821X(73)90195-7

Chung, Y. & Craig, H. (1980). $^{226}$Ra in the Pacific Ocean. *Earth and Planetary Science Letters*, *49*(2), 267–292. https://doi.org/10.1016/0012-821X(80)90072-2

Chung, Y. & Craig, H. (1983). $^{210}$Pb in the Pacific: the GEOSECS measurements of particulate and dissolved concentrations. *Earth and Planetary Science Letters*, *65*(2), 406–432. https://doi.org/10.1016/0012-821X(83)90179-6

Craig, H., Krishnaswami, S. & Somayajulu, B. L. K. (1972). $^{210}$Pb-$^{226}$Ra: radioactive disequilibrium in the deep sea. *Earth and Planetary Science Letters*, *17*(2), 295–305. https://doi.org/10.1016/0012-821X(73)90194-5

Crusius J. & Anderson R.F. (1992). Inconsistencies in accumulation rates of Black Sea sediments inferred from records of laminae and $^{210}$Pb. *Paleoceanography*, *7*(2), 215–227. https://doi.org/10.1029/92PA00279

Danovaro, R., Gambi, C. & Croce, N. D. (2002). Meiofauna hotspot in the Atacama Trench, eastern South Pacific Ocean. *e*, *49*(5), 843–857. https://doi.org/10.1016/S0967-0637(01)00084-X

Danovaro, R., Croce, N. D., Dell'Anno, A. & Pusceddu, A. (2003). A depocenter of organic matter at 7800 m depth in the SE Pacific Ocean. *Deep Sea Research Part I: Oceanographic Research Papers*, *50*(12), 1411–1420. https://doi.org/10.1016/j.dsr.2003.07.001

DeMaster, D. J. & Cochran, J. K. (1982). Particle mixing rates in deep-sea sediments determined from excess $^{210}$Pb and $^{32}$Si profiles. *Earth and Planetary Science Letters*, *61* (2), 257–271. https://doi.org/10.1016/0012-821X(82)90057-7

DeMaster, D. J., McKee, B. A., Nittroer, C. A., Jiangchu, Q. & Guodong, C. (1985). Rates of sediment accumulation and particle reworking based on radiochemieal measurements from continental shelf deposits in the East China Sea. *Continental Shelf Research*, 4, 143–158. https://doi.org/10.1016/0278-4343(85)90026-3

Fuller, C. C., van Geen, A., Baskaran, M. & Anima, R. (1999). Sediment chronology in San Francisco Bay, California, defined by, $^{210}$Pb, $^{234}$Th, $^{137}$Cs and $^{239,240}$Pu. M*arine. Chemistry*, *64*(1–2), 7–27. https://doi.org/10.1016/S0304-4203(98)00081-4

GEBCO Bathymetric Compilation Group (2021). The GEBCO_2021 Grid - a continuous terrain model of the global oceans and land [Dataset]. Global ocean & land terrain models. https://doi.org/10.5285/c6612cbe-50b3-0cff-e053-6c86abc09f8f

Glud R. N., Holby, O., Hoffmann, F. & Canfield, D. E. (1998). Benthic mineralization and exchange in Arctic sediments (Svalbard, Norway). *Marine Ecology Progress Series*, *173*, 237–251. https://doi.org/10.3354/meps173237

Glud R. N., Wenzhöfer, F., Middelboe, M., Oguri, K., Turnewitsch, R., Canfield, D. E. & Kitazato, H. (2013). High rates of microbial carbon turnover in sediments in the deepest oceanic trench on Earth. *Nature Geoscience*, *6*, 284–288. https://doi.org/10.1038/ngeo1773

Glud, R. N., Berg, P., Thamdrup, B., Larsen, M., Stewart, H. A., Jamieson, A. J., et al. (2021). Hadal trenches are dynamic hotspots for early diagenesis in the deep sea. *Communications Earth & Environment*, *2*, 21(2021). https://doi.org/10.1038/s43247-020-00087-2

Harris, P. T., Macmillan-Lawler, M., Rupp, J. & Baker, E. K. (2014). Geomorphology of the oceans. *Marine Geology*, *352*, 4–24. https://doi.org/10.1016/j.margeo.2014.01.011

Heldal, H. E., Helvik, L., Appleby, P., Haans, H., Volynkin, A., Jensen, H. & Lepland, A. (2021). Geochronology of sediment cores from the Vefsnfjord, Norway. Marine *e*, *170*, (2010)112683. https://doi.org/10.1016/j.marpolbul.2021.112683

Hirose, K., Igarashji, & Aoyama, M. (2008). Analysis of the 50-year records of the atmospheric deposition of long-lived radionuclides in Japan. *Applied Radiation and Isotopes*, *66*(11), 1675–1678. https://doi.org/10.1016/j.apradiso.2007.09.019

Hong, G., Kim, S., Chung, C., Kang, D. -J., Shin, D. -H., Lee, H. & Han, S. -J (1997). $^{210}$Pb-derived sediment accumulation rates in the southwestern East Sea (Sea of Japan). *Geo-Marine Letters*, *17*, 126–132. https://doi.org/10.1007/s003670050017

Ichino, M. C., Clark, M. R., Drazen, J. C., Jamieson, A., Jones, D. O., Martin, A. P., et al. (2015). The distribution of benthic biomass in hadal trenches: A modelling approach to investigate the effect of vertical and lateral organic matter transport to the seafloor. *Deep Sea Research Part I: Oceanographic Research Papers*, *100*, 21–33. https://doi.org/10.1016/j.dsr.2015.01.010

Iijima, K., Yasukawa, K., Fujinaga, K., Nakamura, K., Machida, S., Takaya, Y. et al. (2016). Discovery of extremely REY-rich mud in the western North Pacific Ocean. *Geochemical Journal*, *50*, 557–573. https://doi.org/10.2343/geochemj.2.0431

Ikehara, K., Kanamatsu, T., Nagahashi, Y., Strasser, M., Fink, H., Usami, K., et al. (2016). Documenting large earthquakes similar to the 2011 Tohoku-oki earthquake from sediments deposited in the Japan Trench over the past 1500 years. *Earth and Planetary Science Letters*, *445*, 48–56. https://doi.org/10.1016/j.epsl.2016.04.009

Ikehara, K., Usami, K. & Kanamatsu, T. (2020). Repeated occurrence of surface-sediment remobilization along the landward slope of the Japan Trench by great earthquakes. *Earth, Planets and Space*, *72*, 114(2020). https://doi.org/10.1186/s40623-020-01241-y

Ikehara, K., Usami, K., Irino, T., Omura, A., Jenkins, R.G. & Ashi, J. (2021). Characteristics and distribution of the event deposits induced by the 2011 Tohoku-oki earthquake and tsunami offshore of Sanriku and Sendai, Japan. *Sedimentary Geology*, *411*, (2021)105791. https://doi.org/10.1016/j.sedgeo.2020.105791

Itoh, M., Kawamura, K., Kitahashi, T., Kojima, S., Katagiri, H. & Shimanaga, M. (2011). Bathymetric patterns of meiofaunal abundance and biomass associated with the Kuril and Ryukyu trenches, western North Pacific Ocean. *Deep Sea Research Part I: Oceanographic Research Papers*, *58*(1), 86–97. https://doi.org/10.1016/j.dsr.2010.12.004

Itou, M., Matsumura, I., & Noriki, S. (2000). A large flux of particulate matter in the deep Japan Trench observed just after the 1994 Sanriku-Oki earthquake. *Deep Sea Research Part I: Oceanographic Research Papers*, *47*, 1987–1998. https://doi.org/10.1016/S0967-0637(00)00012-1

Kato, Y., Kitazato, H., Shimanaga, M., Nakatsuka, T., Shirayama, Y. & Masuzawa, T. (2003). $^{210}$Pb and $^{137}$Cs in sediments from Sagami Bay, Japan: sedimentation rates and inventories. *Progress in Oceanography*, *57*(1), 77–95. https://doi.org/10.1016/S0079-6611(03)00052-1

Kawamura, K., Sasaki, T., Kanamatsu, T., Sakaguchi, A. & Ogawa, Y. (2012). Large submarine landslides in the Japan Trench: A new scenario for additional tsunami generation, *Geophysical Research Letters*, *39*(5), L05308, https://doi.org/10.1029/2011GL050661

Kioka, A., Schwestermann, T., Moernaut, J., Ikehara, K., Kanamatsu,

T., McHugh, C. et al. (2019a). Megathrust earthquake drives drastic organic carbon supply to the hadal trench. *Scientific Reports*, *9*, 1553(2019), https://doi.org/10.1038/s41598-019-38834-x

Kioka, A., Schwestermann, T., Moernaut, J., Ikehara, K., Kanamatsu, T., Eglinton, T. I. & Strasser, M. (2019b). Event Stratigraphy in a Hadal Oceanic Trench: The Japan Trench as Sedimentary Archive Recording Recurrent Giant Subduction Zone Earthquakes and Their Role in Organic Carbon Export to the Deep Sea. *Frontiers in Earth Science*, *7*, 319(2019), https://doi.org/10.3389/feart.2019.00319

Koide, M., Soutar, A. & Goldberg, E. D. (1972). Marine geochronology with $^{210}$Pb. *Earth and Planetary Science Letters*, *14*(3), 442–446. https://doi.org/10.1016/0012-821X(72)90146-X

Krishnaswami, L. D., Martin, J. M. & Meybeck, M. (1971). Geochronology of lake sediments. *Earth and Planetary Science Letters*, *11*(1–5), 407–414. https://doi.org/10.1016/0012-821X(71)90202-0

Kusakabe, M., Inatomi, N., Takata, H. & Ikenoue, T. (2017). Decline in radiocesium in seafloor sediments off Fukushima and nearby prefectures. *Journal of Oceanography*, *73*, 529–545. https://doi.org/10.1007/s10872-017-0440-2

Luo, M., Giskes, J., Chen, L., Shi, X. & Chen, D. (2017). Provenances, distribution, and accumulation of organic matter in the southern Mariana Trench rim and slope: Implication for carbon cycle and burial in hadal trenches. *Marine Geology*, *386*, 98–106. https://doi.org/10.1016/j.margeo.2017.02.012

Luo, M., Giskes, J., Chen, L., Scholten, J., Pan, B., Lin, G. & Chen, D. (2019). Sources, degradation, and transport of organic matter in the New Britain Shelf-Trench continuum, Papua New Guinea. *Journal of Geophysical Research: Biogeosciences*, *124*, 1680–1695. https://doi.org/10.1029/2018JG004691

Masqué, P., Sanchez-Cabeza, J. A., Bruach, J. M., Palacios, E. & Canals, M. (2002). Balance and residence times of $^{210}$Pb and $^{210}$Po in surface waters of the northwestern Mediterranean Sea. *Continent. Shelf Research*, *22*(15), 2127–2146. https://doi.org/10.1016/S0278-4343(02)00074-2

Masqué, P., Fabres, J., Canals, M., Sanchez-Cabeza, J.A., Vidal-Sanchez, A., Cacho, I., Calafat, A. M. & Bruach, J. M. (2003). Accumulation rates of major constituents of hemipelagic sediments in the deep Alboran Sea: a centennial perspective of sedimentary dynamics. *Marine Geology*, *193*(3–4), 207–233. https://doi.org/10.1016/S0025-3227(02)00593-5

McHugh, C. M., Kanamatsu, T., Seeber, L., Bopp, R., Cormier, M-H, & Usami, K. (2016). Remobilization of surficial slope sediment triggered by the A.D. 2011 $M_w$ 9 Tohoku-Oki earthquake and tsunami along the Japan Trench. *Geology*, *44*(5), 391–394. https://doi.org/10.1130/G37650.1

McHugh, C. M., Seebar, L., Rasbury, T., Strasser, M., Kioka, A., Kanamatsu, T., et al. (2020). Isotopic and sedimentary signature of megathrust

ruptures along the Japan subduction margin. *Marine Geology*, *428*, 106283. https://doi.org/10.1016/j.margeo.2020.106283

Muñoz, P., Lange, C. B., Cutiérrez, D., Hebbeln, D., Salamanca, M. A., Dezileau, L., et al. (2004). Recent sedimentation and mass accumulation rates based on $^{210}$Pb along the Peru-Chile continental margin. *Deep Sea Research Part II: Topical Studies in Oceanography*, *51*(20–21), 2523–2541. https://doi.org/10.1016/j.dsr2.2004.08.015

Nagaya, Y. & Nakamura, K. (1987). Artificial radionuclides in the Western Northwest Pacific (II): $^{137}$Cs and $^{239,\ 240}$Pu inventories in water and sediment columns observed from 1980 to 1986. *Journal of the Oceanographical Society of Japan*, *43*, 345–355. https://doi.org/10.1007/BF02109287

Nittrouer, C. A., DeMaster, D. JK., KcKee, B. A., Cutshall, H. H. & Larsen, L. (1984). The effect of sediment mixing on Pb-210 accumulation rates for the Washington continental shelf. *Marine Geology*, *54*(3–4), 201–221. https://doi.org/10.1016/0025-3227(84)90038-0

Nozaki, Y., Cochran, K., Turekian, K. K. & Keller, G. (1977). Radiocarbon and $^{210}$Pb distribution in submersible-taken deep-sea cores from Project FAMOUS. *Earth and Planetary Science Letters*, *34*(2), 167–173. https://doi.org/10.1016/0012-821X(77)90001-2

Nozaki, Y. (1986). $^{226}$Ra-$^{222}$Rn-$^{210}$Pb systematics in seawater near the bottom of the ocean. *Earth and Planetary Science Letters*, *80*(1–2), 36–40. https://doi.org/10.1016/0012-821X(76)90070-4

Nozaki, Y. & Ohta, Y. (1993). Rapid and frequent turbidite accumulation in the bottom of Izu-Ogasawara Trench: Chemical and radiochemical evidence. *Earth and Planetary Science Letters*, *120*(3–4), 345–360. https://doi.org/10.1016/0012-821X(93)90249-9

Nozaki, Y., Zhang, J. & Takeda, A. (1997). $^{210}$Pb and $^{210}$Po in the equatorial Pacific and the Bering Sea: the effects of biological productivity and boundary scavenging. *Deep Sea Research Part II: Topical Studies in Oceanography*, *44*(9–10), 2203–2220. https://doi.org/10.1016/S0967-0645(97)00024-6

Nozaki, Y., Yamada, M., Nakanishi, T., Nagaya, Y., Nakamura, K., Shitashima, K. & Tsubota, H. (1998). The distribution of radionuclides and some trace metals in the water columns of the Japan and Bonin trenches. *Oceanologica Acta*, *21*(3), 469–484. https://doi.org/10.1016/S0399-1784(98)80031-5

Oguri, K., Matsumoto, E., Saito, Y., Yamada, M. & Iseki, K. (2003). Sediment accumulation rates and budgets of depositing particles of the East China Sea. *Deep Sea Research Part II: Topical Studies in Oceanography*, *50*(2), 513–528. https://doi.org/10.1016/S0967-0645(02)00465-4

Oguri, K., Harada, N. & Tadai, O. (2012). Excess $^{210}$Pb and $^{137}$Cs concentrations, mass accumulation rates, and sedimentary processes on the Bering Sea

continental shelf. *Deep Sea Research Part II: Topical Studies in Oceanography*, *61–64*, 193–204. https://doi.org/10.1016/j.dsr2.2011.03.007

Oguri, K., Kawamura, K., Sakaguchi, A., Toyofuku, T., Kasaya, T., Murayama, M., et al. (2013). Hadal disturbance in the Japan Trench induced by the 2011 Tohoku-Oki Earthquake. *Scientific Reports*, *3*, 1915 (2013), https://doi.org/10.1038/srep01915

Oguri, K., Furushima, Y., Toyofuku, T., Kasaya, T., Wakita, M., Watanabe, S., Fujikura, K., Kitazato, H. (2016). Long-term monitoring of bottom environments of the continental slope off Otsuchi Bay, northeastern Japan. *Journal of Oceanography*, *72*, 151–166. https://doi.org/10.1007/s10872-015-0330-4

Radakovitch, O. & Heussner (1999). Fluxes and budget of $^{210}$Pb on the continental margin of the Bay of Biscay (northeastern Atlantic). *Deep Sea Research Part II: Topical Studies in Oceanography*, *46*(10), 2175–2203. https://doi.org/10.1016/S0967-0645(99)00059-4

Reimers, C. E., Jahnke, R. A. & McCorkle, D. C. (1992). Carbon fluxes and burial rates over the continental slope and rise off central California with implications for the global carbon cycle. *Global Biogeochemical Cycles*, *6*(2), 199–224.https://doi.org/10.1029/92GB00105

Sanchez-Cabeza, J. A., Masqué, P. & Ani-Ragolta, I. (1998). $^{210}$Pb and $^{210}$Po analysis in sediments and soils by microwave acid digestion. *Journal of Radioanalytical and Nuclear Chemistry*, *227*, 19–22. https://doi.org/10.1007/bf02386425

Sanchez-Cabeza, J. A., Masqué, P, Ani-Ragolta, I., Merino, J., Frignani, M., Alvisi, F., Palanques, A. & Puig, P. (1999). Sediment accumulation rates in the southern Barcelona continental margin (NW Mediterranean Sea) derived from $^{210}$Pb and $^{137}$Cs Chronology. *Progress in Oceanography*, *44*, 313–332. https://doi.org/10.1016/S0079-6611(99)00031-2

Schauberger, C., Middelboe, M., Larsen, M., Peoples, L., M., Bartlett, D. H., Kirpejear, F., et al. (2021). Spatial variability of prokaryotic and viral abundances in the Kermadec and Atacama Trench regions. *Limnology and Oceanography*, *66*(6), 2095–2109. https://doi.org/10.1002/lno.11711

Stewart, H.A., & Jamieson, A.J. (2018). Habitat heterogeneity of hadal trenches: considerations and implications for future studies. *Progress in Oceanography*, *161*, 47–65. https://doi.org/10.1016/j.pocean.2018.01.007

Thomson, J. & Turekian, K. K. (1976). $^{210}$Po and $^{210}$Pb distributions in ocean water profiles from the eastern south Pacific. *Earth and Planetary Science Letters*, *32*(2), 297–303. https://doi.org/10.1016/0012-821X(76)90069-8

Tsumune, D., Aoyama, M., Hirose, K., Bryan, F. O., Lindsay, K. & Danabasoglu, G. (2011). Transport of $^{137}$Cs to the Southern Hemisphere in an ocean general circulation model. *Progress in Oceanography*, *89*(1–4), 38–48. https://doi.org/10.1016/j.pocean.2010.12.006

Turnewitsch, R., Reyss, J-L., Chapman, D.C., Thomson, J. & Lampitt, R.S. (2004). Evidence for a sedimentary fingerprint of an asymmetric flow surrounding a short seamount. *Earth and Planetary Science Letters*, *222*(3–4), 1023–1036. https://doi.org/10.1016/j.epsl.2004.03.042

Turnewitsch, R., Falahat, S., Stehjjlikova, J., Oguri, K., Glud, R. N., Middelboe, M., et al. (2014). Recent sediment dynamics in hadal trenches: Evidence for the influence of higher-frequency (tidal, near-intertidal) fluid dynamics. *Deep Sea Research Part I: Oceanographic Research Papers*, *90*, 125–138. https://doi.org/10.1016/j.dsr.2014.05.005

Usami, K., Ikehara, K., Kanamatsu, T. & McHugh, C.M. (2018). Supercycle in great earthquake recurrence along the Japan Trench over the last 4000 years. *Geoscience Letters*, *5*, 11(2018). https://doi.org/10.1186/s40562-018-0110-2

Usami, K., Ikehara, K., Kanamatsu, T., Kioka, A., Schwestermann, T. & Strasser, M. (2021). The Link Between Upper-Slope Submarine Landslides and Mass Transport Deposits in the Hadal Trenches. Understanding and Reducing Landslide Disaster Risk. In *Understanding and Reducing Landslide Disaster Risk. Volume 1 Sendai Landslide Partnerships and Kyoto Landslide Commitment* (pp.361-367). Springer Nature Switzerland AG.

van Haren, H. (2020). *Deep Sea Research Part I: Oceanographic Research Papers*, *165*, 103400. https://doi.org/10.1016/j.dsr.2020.103400

Wenzhöfer, F., Oguri, K., Middelboe, M., Turnewitsch, R., Toyofuku, T., Kitazato, H. & Glud, R. N. (2016). Benthic carbon mineralization in hadal trenches: Assessment by in situ $O_2$ microprofile measurements. *Deep Sea Research Part I: Oceanographic Research Papers*, *116*, 276–286. https://doi.org/10.1016/j.dsr.2016.08.013

Xu, Y., Li, X., Luo, M., Xiao, W., Fang, J., Rashid, H., et al. (2021). Distribution, source and burial of sedimentary organic carbon in Kermadec and Atacama trenches. *Journal of Geophysical Research: Biogeosciences*, 126, e2020JG006189. https://doi.org/10.1029/2020JG006189

Yeager, K. M., Santschi, P. H. & Rowe, G. T. (2004). Sediment accumulation and radionuclide inventories ($^{239,240}$Pu, $^{210}$Pb and $^{234}$Th) in the northern Gulf of Mexico, as influenced by organic matter and macrofaunal density. *Marine Chemistry*, *91*, 1–14. https://doi.org/10.1016/j.marchem.2004.03.016

Zhang, X., Xu, Y., Xiao, W., Zhao, M., Wang, Z., Wang, X. et al. (2022). The hadal zone is an important and heterogeneous sink of black carbon in the oceans. *Communications Earth & Environment*, *in press.*